Journal of Computational Physics 315 (2016) 1–15

Contents lists available at ScienceDirect

Journal of Computational Physics

www.elsevier.com/locate/jcp

Lattice Boltzmann modeling of phonon transport

Yangyu Guo, Moran Wang *

Department of Engineering Mechanics and CNMM, Tsinghua University, Beijing 100084, China

ARTICLE INFO

Article history:
Received 24 July 2015
Received in revised form 22 December 2015
Accepted 19 March 2016
Available online 23 March 2016

Keywords:
Phonon transport
Lattice Boltzmann model
Chapman–Enskog expansion
Phonon hydrodynamics

ABSTRACT

A novel lattice Boltzmann scheme is proposed for phonon transport based on the phonon Boltzmann equation. Through the Chapman–Enskog expansion, the phonon lattice Boltzmann equation under the gray relaxation time approximation recovers the classical Fourier's law in the diffusive limit. The numerical parameters in the lattice Boltzmann model are therefore rigorously correlated to the bulk material properties. The new scheme does not only eliminate the fictitious phonon speed in the diagonal direction of a square lattice system in the previous lattice Boltzmann models, but also displays very robust performances in predicting both temperature and heat flux distributions consistent with analytical solutions for diverse numerical cases, including steady-state and transient, macroscale and microscale, one-dimensional and multi-dimensional phonon heat transport. This method may provide a powerful numerical tool for deep studies of nonlinear and nonlocal heat transports in nanosystems.

1. Introduction

Heat transport mediated by phonon is an important topic in fundamental thermal physical science [1,2] and has wide technology applications in semiconductor and microelectronics industries, thermo-electronics and functional nanomaterials [3,4]. There are mainly three categories of theoretical methods to model the phonon transport in view of descriptions at different levels: microscopic, mesoscopic and macroscopic methods [5]. Molecular dynamic simulation [6,7] is a typical microscopic method, which provides the information of all the particles making up the solid. It is computational intensive and time-consuming, and usually applied to model phonon transport in extremely small structures. Mesoscopic method describes the phonon transport by a single-particle distribution function governed by Boltzmann equation [8]. A more coarse-grained description is the macroscopic method, which uses merely several statistical averaging variables (moments of the single-particle distribution function). The most classical one is the Fourier's law [9], which gives a linear dependence of heat flux on the temperature gradient. It is appreciably valid and widely applied in conventional engineering situations where heat transports in the so-called diffusive regime [1,2,4,5]. However, as the temporal and spatial scales reduce to be comparable to or smaller than the relaxation time and mean free path of phonons, the Fourier's law becomes no longer available [1,3,6,10]. To remedy this situation, Cattaneo–Vernotte (C–V) model [11,12] was proposed to account the temporal relaxation effect, resulting in the propagation of heat waves [10,13,14]. But to the author's best knowledge, the C–V model is not able to describe any actual phonon transport processes yet to date [15]. Macroscopic methods beyond the C–V model were thus developed, such as the phonon hydrodynamics model [5,16,17] and so on [18]. They consider the spatial nonlocal effects besides the temporal relaxation effect in micro- and nanoscale. Thus it becomes credible to model phonon transport

* Corresponding author. Tel.: +86 10 627 87498.
E-mail address: mrwang@tsinghua.edu.cn (M. Wang).

http://dx.doi.org/10.1016/j.jcp.2016.03.041
0021-9991/

in simple nanoscale geometries such as thin films, nanowires and nanotubes [5,16,19,20]. But the rigorous development of widely applicable macroscopic models for nanoscale heat transport remains still an open question [5].

To tackle phonon transport in a wide range of temporal and spatial scales, solution of phonon Boltzmann equation is required. But it is a big challenge due to the intractable collision term and nonlinear phonon dispersion relation [1,2,8]. Monte Carlo (MC) method [21] is a popular approach, supplemented with phonon information (collision rates, dispersion relation, etc.) obtained from first-principle calculations or molecular dynamic simulations [7,22]. However, MC simulation is born with stochastic statistical uncertainty, and is inefficient to implement in complicated geometries [21]. In comparison, lattice Boltzmann method is a promising method inherited with natural mesoscopic foundation, high efficiency of parallel computations and easy treatments with complex geometries [23,24]. It was proposed for simulating hydrodynamics based on the rigorous relation between lattice Boltzmann equation and Navier–Stokes equations [25–27], and was widely extended to numerical modeling of various transport phenomena [28–32]. In recent years, the lattice Boltzmann scheme is introduced to solve the phonon Boltzmann equation [33–35]. Steady-state and transient phonon transport problems have been simulated by different phonon lattice Boltzmann models [36–47].

However, there are still several essential issues to be clarified for the existing phonon lattice Boltzmann methods: (*i*) value of the lattice speed, (*ii*) lattice weights of the equilibrium distribution, (*iii*) central-point component of lattice. As is well known that the lattice speed is different in definition from the group speed; therefore generally the value of lattice speed also differs from that of group speed. However this value was often assumed same as that of phonon group speed [33–39,41–43,45,47], which could be valid only for very special cases (such as the isotropic D3Q7 lattice). Besides, empirical values were adopted without any physical basis sometimes for the lattice speed [40,44,46] and for the lattice weights of equilibrium distributions as well [35,41,46]. Just referring the classical lattice Boltzmann models for hydrodynamics, some studies applied a non-zero central-point component for the lattice systems for phonon [43–45], which may be inappropriate because the phonon is a kind of pseudo particle, different from real fluid molecules, owning no static mass for lingering. The empirical values for lattice speed and lattice weights therefore brought in the fictitious phonon speed in the diagonal direction of a D2Q9 lattice scheme [40,46,48]. To avoid the deficiency of D2Q9 lattice, a triangular (D2Q7) lattice was proposed to be more applicable in 2D simulations [40]. Nevertheless, the complex boundary treatments in D2Q7 lattice restricted its applications, and it was difficult to extend to three-dimensional cases.

Actually all these inconsistencies result from the absent connection between mesoscopic numerical scheme and macroscopic physics of phonon transport. The numerical parameters in the previous lattice Boltzmann models were usually determined empirically rather than correlated rigorously to the bulk material properties. As a result, the predictions often met incorrect or inexplainable cross-section profiles of heat flux for steady-state cases [39,40,43–45] or of both temperature and heat flux for transient ones [40,44,47].

Therefore, the present work is to establish the relation between numerical parameters and bulk material properties through a rigorous Chapman–Enskog expansion solution of the phonon lattice Boltzmann equation. The remainder of this article is organized as below: in Section 2, the mathematical and numerical methods will be introduced, including the phonon Boltzmann equation, the new scheme of phonon lattice Boltzmann equation and its recovery to macroscopic heat transport equations, and the details of boundary treatments; in Section 3, several numerical cases are used to test the performance of the new lattice Boltzmann model; the concluding remarks are finally summarized in Section 4.

2. Mathematical and numerical methods

In this section, the phonon lattice Boltzmann equation is introduced from the Boltzmann equation in the kinetic theory of phonons. The solution to lattice Boltzmann equation is conducted by a Chapman–Enskog expansion. Macroscopic heat transport equations are recovered in the diffusive limit, and the correlations between numerical parameters and bulk material properties are established for 1D, 2D and 3D situations respectively. Finally, the treatments of several types of boundary conditions for the lattice Boltzmann scheme are provided.

2.1. Phonon Boltzmann equation

Phonon Boltzmann equation describes the balance between variation, advection and scattering of phonons [8]:

$$\frac{\partial f}{\partial t} + \mathbf{v}_g \cdot \nabla f = C(f), \tag{1}$$

where $f \equiv f(\mathbf{x}, t, \mathbf{k})$ is the phonon distribution function, with $f(\mathbf{x}, t, \mathbf{k})d\mathbf{x}d\mathbf{k}$ denoting the number of phonons within the spatial interval ($\mathbf{x}$, $\mathbf{x}+d\mathbf{x}$) and wave vector interval ($\mathbf{k}$, $\mathbf{k}+d\mathbf{k}$) at a specific time t. The wave vector $\mathbf{k}$ is an extension of wave number (the reciprocal of wave length), and is related to the phonon group velocity $\mathbf{v}_g$ and phonon frequency ω through the dispersion relation $\mathbf{v}_g = \nabla_{\mathbf{k}}\omega$. The intractable collision term is usually treated by the relaxation time approximation [1,2]:

$$C(f) = -\frac{f - f^{eq}}{\tau_R(\omega)}. \tag{2}$$

As the first step, the Debye's linear dispersion relation and gray approximation are assumed in the present work. In this way, the phonon group speed v_g becomes a constant, and the relaxation time τ_R is frequency independent. Under these approximations, Eq. (1) becomes:

$$\frac{\partial f}{\partial t} + \mathbf{v}_g \cdot \nabla f = -\frac{f - f^{eq}}{\tau_R}, \tag{3}$$

with the Planck equilibrium distribution [1]:

$$f^{eq} = \frac{1}{\exp(\hbar\omega/k_B T) - 1}, \tag{4}$$

with $\hbar = h/2\pi$ the reduced Planck constant, k_B the Boltzmann constant. For convenience, Eq. (3) is usually reformulated into the energy form [36,39]:

$$\frac{\partial e}{\partial t} + \mathbf{v}_g \cdot \nabla e = -\frac{e - e^{eq}}{\tau_R}. \tag{5}$$

The phonon energy density is defined as $e \equiv \int f \hbar\omega D(\omega) d\omega$, with $D(\omega)$ the phonon state density function, and the equilibrium phonon energy density is $e^{eq} \equiv \int f^{eq} \hbar\omega D(\omega) d\omega$.

2.2. Phonon lattice Boltzmann equation

In analogy to the derivation of the lattice Boltzmann equation for hydrodynamics [23,27], the phonon lattice Boltzmann equation is obtained as a discrete form of the phonon Boltzmann equation Eq. (5) [36,39,46]:

$$\frac{\partial e_i(\mathbf{x}, t)}{\partial t} + \mathbf{c}_i \cdot \nabla e_i(\mathbf{x}, t) = -\frac{e_i(\mathbf{x}, t) - e_i^{eq}(\mathbf{x}, t)}{\tau_R}, \tag{6}$$

where $\mathbf{c}_i$ $(i = 1, 2, 3, \ldots, n)$ are the discrete lattice velocities, and n is the number of them. The temporal and spatial derivatives of $e_i(\mathbf{x}, t)$ at the left side of Eq. (6) are approximated by the first-order difference, thus Eq. (6) becomes:

$$\frac{e_i(\mathbf{x} + \mathbf{c}_i \Delta t, t + \Delta t) - e_i(\mathbf{x}, t)}{\Delta t} = -\frac{e_i(\mathbf{x}, t) - e_i^{eq}(\mathbf{x}, t)}{\tau_R}, \tag{7}$$

which results in the phonon lattice Boltzmann equation:

$$e_i(\mathbf{x} + \mathbf{c}_i \Delta t, t + \Delta t) - e_i(\mathbf{x}, t) = -\frac{e_i(\mathbf{x}, t) - e_i^{eq}(\mathbf{x}, t)}{\tau}. \tag{8}$$

The non-dimensional relaxation time is $\tau = \tau_R/\Delta t$, with Δt the lattice time step, related to the spatial step by $\Delta \mathbf{x} = \mathbf{c}_i \Delta t$. The discrete equilibrium phonon energy densities are assumed to be identical [36,39,40,46]:

$$e_i^{eq} = \frac{1}{n} e^{eq} = \frac{1}{n} \int f^{eq} \hbar\omega D(\omega) d\omega. \tag{9}$$

Under the Debye's approximation assumed in the present work, the equilibrium phonon energy density becomes [1]:

$$e^{eq} = \frac{9 N k_B T}{V} \left(\frac{T}{\Theta_D}\right)^3 \int_0^{\Theta_D/T} \frac{x^3}{\exp(x) - 1} dx, \tag{10}$$

with N/V the number density of crystal atoms, Θ_D the Debye temperature and the dimensionless variable $x \equiv \hbar\omega/k_B T$. Theoretically, the local temperature of a crystal must be determined through an inverse numerical integration from the local phonon energy density based on Eq. (10) [36]. However, this inverse computation is complex and only necessary for extremely low temperature ($T \ll \Theta_D$) situation where the temperature dependence of heat capacity is prominent. In the present work, for mathematical simplicity and clear interpretation of the main points, we consider the limit of high temperature where the heat capacity approaches a constant such that Eq. (10) reduces to $e^{eq} \simeq C_V T$, with C_V the heat capacity per unit volume. Therefore, Eq. (9) becomes:

$$e_i^{eq} = \frac{1}{n} e^{eq} = \frac{1}{n} C_V T, \tag{11}$$

which is actually often adopted in previous phonon LBM models [44,46]. Incorporation of Eq. (10) into the present numerical model is trivial, which could be taken into account when necessary.

Finally a comparison is clarified between the equilibrium distribution functions of phonon LBM and of classical LBM for hydrodynamics. In classical LBM, the discrete equilibrium distribution function is derived from the local Maxwell–Boltzmann distribution, which describes the probability of finding particles in velocity space. Thus the discrete lattice velocities with different weights are designed to model the mesoscopic kinetics of particles in order to recover the macroscopic hydrodynamics. In contrast, under the usual Debye's approximation made in phonon LBM, the phonon group velocities have an identical value in different directions, i.e. a uniform velocity space. The equilibrium distribution function of phonons

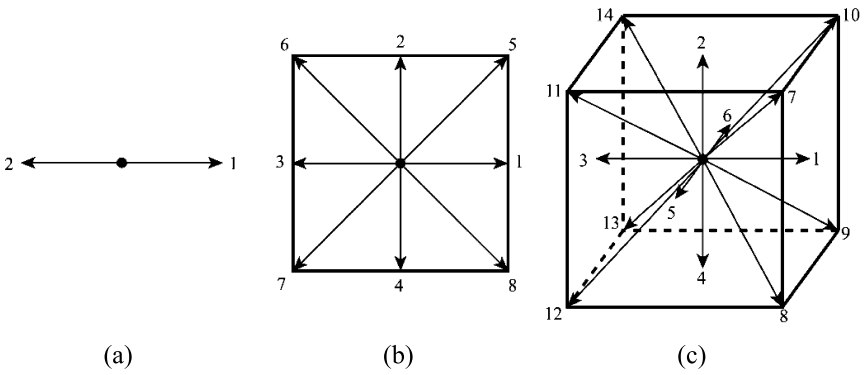

Fig. 1. Lattice structures for phonon lattice Boltzmann model at different dimensions: (a) D1Q2, (b) D2Q8, (c) D3Q14.

is the Bose–Einstein distribution (Planck distribution), which describes the probability of finding pseudo particles in frequency space. Since the evolution of phonon energy density is considered in the present LBM, the frequency dependence is avoided. Thus the discrete equilibrium function Eq. (9) essentially denotes a probability distribution of energy in the directional space. This explains why the identical weights are often used in the hitherto proposed LBM for modeling phonon transport in isotropic materials. A direct evolution of the frequency-dependent phonon distribution function in LBM remains still an open challenge. The similar problem is unresolved in LBM solution of photon (radiative) transfer [32] since both photon and phonon are bosons.

2.3. Chapman–Enskog expansion

To recover the macroscopic heat transport equation, Chapman–Enskog expansion is applied to solve the phonon lattice Boltzmann equation Eq. (8). Lattice structures including D1Q2, D2Q8 and D3Q14 are considered, as shown in Fig. 1. The central-point component with vanishing lattice velocity is not counted here, which is the main distinction from the lattice Boltzmann model for hydrodynamics. This distinction originates in that the conservation laws of particle number and mass in hydrodynamics are no longer ensured in phonon transport [1,2]. On the other hand, since phonon is a kind of boson with zero static mass, its velocity can never reach zero, otherwise it will disappear. The typical D2Q8 lattice will be used as an example for the Chapman–Enskog expansion, which can be done through similar procedures for other lattice structures.

A Taylor expansion of $e_i(\mathbf{x}+\mathbf{c}_i\Delta t, t+\Delta t)$ is conducted around $e_i(\mathbf{x},t)$ within second order since the lattice time step is usually small:

$$e_i(\mathbf{x}+\mathbf{c}_i\Delta t, t+\Delta t) = e_i(\mathbf{x},t) + \Delta t\left(\frac{\partial}{\partial t} + c_{i\alpha}\frac{\partial}{\partial x_\alpha}\right)e_i(\mathbf{x},t) + \frac{1}{2}(\Delta t)^2\left(\frac{\partial}{\partial t} + c_{i\alpha}\frac{\partial}{\partial x_\alpha}\right)^2 e_i(\mathbf{x},t). \tag{12}$$

Substitution of Eq. (12) into Eq. (8) gives rise to:

$$\left(\frac{\partial}{\partial t} + c_{i\alpha}\frac{\partial}{\partial x_\alpha}\right)e_i(\mathbf{x},t) + \frac{1}{2}\Delta t\left(\frac{\partial}{\partial t} + c_{i\alpha}\frac{\partial}{\partial x_\alpha}\right)^2 e_i(\mathbf{x},t) = -\frac{e_i(\mathbf{x},t) - e_i^{\mathrm{eq}}(\mathbf{x},t)}{\tau_{\mathrm{R}}}. \tag{13}$$

Two time scales t_1 and t_2, and one spatial scale $\mathbf{x}_1$ [23,24,27] are introduced such that $\partial/\partial x_\alpha = \varepsilon\partial/\partial x_{1\alpha}$, $\partial/\partial t = \varepsilon\partial/\partial t_1 + \varepsilon^2\partial/\partial t_2$, with ε a small parameter often chosen as the Kn number defined as the ratio of phonon mean free path l to system characteristic size L [23,49]. The discrete phonon energy densities are asymptotically expanded within first order: $e_i(\mathbf{x},t) = e_i^{(0)}(\mathbf{x},t) + \varepsilon e_i^{(1)}(\mathbf{x},t) + \cdots$. Putting these expressions into Eq. (13), we achieve the subsequent orders of magnitude on ε^0, ε^1, ε^2 respectively:

$$e_i^{(0)}(\mathbf{x},t) = e_i^{\mathrm{eq}}(\mathbf{x},t), \tag{14}$$

$$\frac{\partial e_i^{(0)}(\mathbf{x},t)}{\partial t_1} + c_{i\alpha}\frac{\partial e_i^{(0)}(\mathbf{x},t)}{\partial x_{1\alpha}} = -\frac{1}{\tau_{\mathrm{R}}}e_i^{(1)}(\mathbf{x},t), \tag{15}$$

$$\frac{\partial e_i^{(0)}(\mathbf{x},t)}{\partial t_2} + \left(1-\frac{1}{2\tau}\right)\frac{\partial e_i^{(1)}(\mathbf{x},t)}{\partial t_1} + \left(1-\frac{1}{2\tau}\right)c_{i\alpha}\frac{\partial e_i^{(1)}(\mathbf{x},t)}{\partial x_{1\alpha}} = 0. \tag{16}$$

The conservation law of phonon energy is ensured during the collision process, thus: $\sum_i e_i = \sum_i e_i^{\mathrm{eq}}$, which results in $\sum_i e_i^{(r)} = 0$ for $r \geq 1$ when combined with the asymptotic expression of $e_i(\mathbf{x},t)$ and Eq. (14). The heat flux $\mathbf{q}$ is also asymptotically expanded within first order: $q_\alpha(\mathbf{x},t) = q_\alpha^{(0)}(\mathbf{x},t) + \varepsilon q_\alpha^{(1)}(\mathbf{x},t) + \cdots$. Conducting a summation over i of Eq. (15) and Eq. (16) respectively, and then combining the two equations in terms of the temporal and spatial scales t_1, t_2 and $\mathbf{x}_1$ gives rise to the energy balance equation:

Table 1
Correlations between lattice speeds and phonon group speed.

Lattice structures	Discrete lattice velocities	Lattice speed
D1Q2	$(\pm1,0,0)c$	$c=\frac{1}{\sqrt{3}}v_g$
D2Q8	$(\pm1,0,0)c,(0,\pm1,0)c,(\pm1,\pm1,0)c$	$c=\frac{2}{3}v_g$
D3Q14	$(\pm1,0,0)c,(0,\pm1,0)c,(0,0,\pm1)c,(\pm1,\pm1,\pm1)c$	$c=\sqrt{\frac{7}{15}}v_g$

$$\frac{\partial e}{\partial t'}+\frac{\partial q_\alpha}{\partial x_\alpha}=0, \tag{17}$$

with the realistic time scale t' related to the time scale t in lattice Boltzmann model by $t'=(1-1/2\tau)t$. The concerning macroscopic variables: local temperature and heat flux are computed from the discrete phonon energy density through: $e=\sum_i e_i=C_V T$ and $q_\alpha(\mathbf{x},t)=\sum_i c_{i\alpha}e_i(\mathbf{x},t)$. Multiplying $\mathbf{c}_i$ on both sides of Eq. (15) and Eq. (16), then conducting a summation over i respectively, and finally combining the two equations gives rise to the heat transport equation:

$$q_\alpha=-\frac{3}{4}\tau_R c^2\frac{\partial e}{\partial x_\alpha}. \tag{18}$$

Eq. (18) is nothing but the classical Fourier's law: $q_\alpha=-\lambda\partial T/\partial x_\alpha$ since $de=C_V dT$. This equivalence, supplemented with the kinetic expression of thermal conductivity $\lambda=C_V\tau_R v_g^2/3$ [2], gives the relation between the lattice speed and phonon group speed:

$$c=\frac{2}{3}v_g. \tag{19}$$

Therefore, the Fourier's law is recovered through the Chapman–Enskog expansion solution of phonon lattice Boltzmann equation. The above expansion is within first-order, but the lattice Boltzmann scheme has a second order accuracy [27]. The lattice speed is not identical to but correlated to the phonon group speed by Eq. (19), which ensures an accurate capturing of the macroscopic behaviors of phonons based on the mesoscopic simulation. Through similar procedures, Chapman–Enskog expansion is conducted for D1Q2 and D3Q14 lattice structures, and the Fourier's law is also recovered with the relations between lattice speed and phonon group speed obtained. The three different types of lattice structures and the corresponding lattice speeds are summarized thoroughly in Table 1. This is in strong contrast to most of previous work [34,36,39,43] where the phonon group speed was taken as the lattice speed, and a recent work [40] where the lattice speed assumed an average projected phonon speed computed as $\frac{1}{2\pi}\int_0^\pi v_g\sin\theta\sin\varphi\int_0^\pi\sin\theta d\theta d\varphi=\frac{v_g}{2}$ for one-dimensional transport whereas $\frac{1}{\pi}\int_0^\pi v_g\sin\theta d\theta=\frac{2}{\pi}v_g$ for two-dimensional transport, which are later adopted in Refs. [44,46]. Here θ,φ are respectively the zenith and azimuthal angles in spherical coordinate system. The projected phonon speed has an unclear physical interpretation, thus is an empirical rather than rigorous value for the lattice speed.

2.4. Boundary treatments

The treatments of isothermal, isoflux, and adiabatic boundary conditions for the present lattice Boltzmann scheme are provided in this part. In addition, a periodic temperature gradient boundary condition is introduced to deal with the situation where heat transports in a region with large length–width ratio.

The D2Q8 lattice is again taken as an example to illustrate the details of boundary treatments. The treatments of isothermal, isoflux and adiabatic boundaries are shown in Fig. 2. The isothermal boundary condition is implemented by dividing equally the equilibrium phonon energy density prescribed by the wall temperature into each lattice components:

$$e_i=\frac{1}{8}e^{eq}=\frac{1}{8}C_V T_{eq}\quad(i=1,2,\ldots,8). \tag{20}$$

Isoflux boundary condition is implemented by inversely calculating the unknown lattice components from the inflowing wall flux q_0 and the known lattice components after the propagation step:

$$e_{4,7,8}=\frac{1}{3}\left[\frac{q_0}{c}+(e_2+e_5+e_6)\right]. \tag{21}$$

Adiabatic boundary condition is set based on the diffuse scheme which divides equally the summation of known incident lattice components into the unknown reflected lattice components:

$$e_{2,5,6}=\frac{1}{3}(e_4+e_7+e_8). \tag{22}$$

A periodic temperature gradient boundary condition shown in Fig. 3 is introduced to exert a constant temperature gradient $(T_L-T_R)/L$ along the transport region [46]. The unknown lattice components of phonon energy density at the

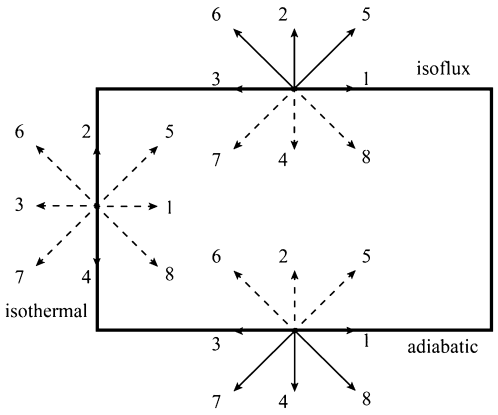

Fig. 2. Schematic for numerical implementation of boundary conditions (isothermal, isoflux and adiabatic) of the phonon lattice Boltzmann model. The solid-line arrow represents the known lattice components whereas dashed-line arrow represents the unknown ones after the propagation step.

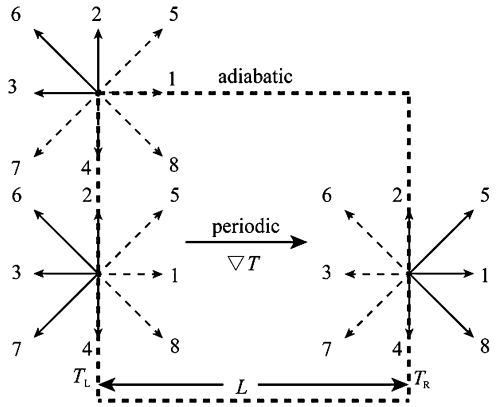

Fig. 3. Schematic for numerical implementation of periodic temperature gradient boundary in the phonon lattice Boltzmann model. The solid-line arrow represents the known lattice components whereas dashed-line arrow represents the unknown ones after the propagation step.

left-side (L) wall and at the right-side (R) wall are respectively got based on the identical deviations from the equilibrium distributions at both sides:

$$e_{1,5,8}(\mathrm{L}) = e^{\mathrm{eq}}_{1,5,8}(\mathrm{L}) + e_{1,5,8}(\mathrm{R}) - e^{\mathrm{eq}}_{1,5,8}(\mathrm{R}), \tag{23}$$

$$e_{3,6,7}(\mathrm{R}) = e^{\mathrm{eq}}_{3,6,7}(\mathrm{R}) + e_{3,6,7}(\mathrm{L}) - e^{\mathrm{eq}}_{3,6,7}(\mathrm{L}). \tag{24}$$

The equilibrium phonon energy densities in Eq. (23) and Eq. (24) are prescribed by the wall temperature at the left side and right side separately based on Eq. (20). Eq. (23) and Eq. (24) are actually inspired from a similar treatment of periodic heat flux boundary in Monte Carlo solution of phonon Boltzmann equation [50]. The identical deviations will induce identical temperature gradients at the two sides, since a distortion of the phonon distribution function from its equilibrium counterpart means a local nonequilibrium temperature gradient. Special care should be put on the treatment of corner point, for instance, the cross point of periodic temperature gradient boundary and adiabatic boundary. Firstly the unknown lattice components e_1, e_5 are set by Eq. (23), and then the unknown lattice components e_4, e_7, e_8 are obtained based on the diffuse scheme Eq. (22) for adiabatic boundary.

3. Numerical results and discussion

In this section, several classical numerical cases are simulated to test the new lattice Boltzmann scheme. They include 1D transient phonon transport, 2D steady-state phonon transport, 3D steady-state phonon transport, in-plane and cross-plane phonon transport through thin films. The in-plane and cross-plane phonon transport spreads a wide range from macroscale to microscale. Throughout all these simulations, the phonon transport is studied in silicon materials at around 300 K, of which the bulk thermal properties are listed in Table 2 [40]. To ensure the constant properties, small temperature differences are considered as in previous work. Relatively large temperature differences have been tested at constant properties, where the present scheme still gives stable and accurate results. Nonlinear problems with temperature-dependent properties will be investigated in future work.

Table 2
Thermal properties of bulk silicon at 300 K.

Properties	Values	Units
Thermal conductivity (λ)	148	W/m K
Volumetric specific heat (C_V)	1.66×10^6	J/m^3 K
Phonon mean free path (l)	41.79	nm
Phonon group speed (v_g)	6400	m/s
Phonon relaxation time (τ_R)	6.53×10^{-12}	s

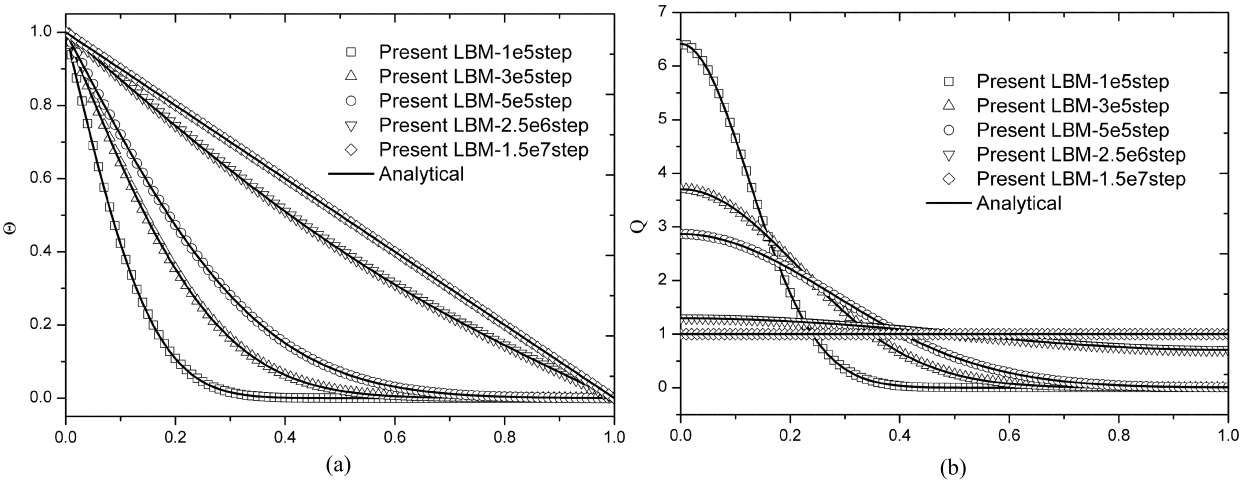

Fig. 4. Non-dimensional temperature and heat flux distributions in 1D transient phonon transport at different time: (a) temperature; (b) heat flux at 1×10^5, 3×10^5, 5×10^5, 2.5×10^6 and 1.5×10^7 lattice time steps. Symbols represent the numerical results by the present LBM, and solid lines represent the analytical results by Eq. (25).

3.1. One-dimensional transient phonon transport

1D transient phonon transport is simulated through a silicon medium initially at a uniform temperature $T_0 = 299.9$ K, with a sudden temperature rise at the left (L) side such that $T_L = 300.1$ K at the initial instant $t' = 0$. The length of the medium is L, and the $Kn = l/L$ is set to be 0.001 in the diffusive regime. The D1Q2 lattice with a lattice speed $v_g/\sqrt{3}$ is used, with a grid number of 1001 after grid independence verification.

The temporal evolutions of temperature and heat flux distributions in this 1D transient heat conduction can be obtained through an analytical solution of the heat diffusion equation (as a combination of Eq. (17) and Eq. (18)) by the method of variable separation [51]:

$$\Theta \equiv \frac{T - T_0}{T_L - T_0} = 1 - X - \frac{2}{\pi}\sum_{n=1}^{\infty}\frac{1}{n}\sin(n\pi X)\exp\left(-Kn\frac{n^2\pi^2\xi}{3}\right)$$
$$Q \equiv \frac{Lq}{\lambda(T_L - T_0)} = 1 + 2\sum_{n=1}^{\infty}\cos(n\pi X)\exp\left(-Kn\frac{n^2\pi^2\xi}{3}\right), \tag{25}$$

where the non-dimensional spatial and temporal coordinates are respectively defined as:

$$X = \frac{x}{L}, \qquad \xi = \frac{t'}{\tau_R}Kn. \tag{26}$$

The numerical results of the temporal evolutions of temperature and heat flux distributions by the present lattice Boltzmann scheme are shown in Fig. 4(a) and Fig. 4(b) respectively. The temperature rise at the left side gradually propagates into the medium in a diffusive way. A linear temperature distribution and uniform heat flux distribution are finally reached. It is seen that they agree well with the analytical solutions. Note that it is crucial to correlate the time scale in the present lattice Boltzmann model with the realistic time scale by $t' = (1 - 1/2\tau)t$ in order to capture accurately the transient behaviors in phonon transport. Incorrect temporal evolutions of both temperature and heat flux distributions would be obtained, as in Refs. [40,44,47], where this correlation rigorously derived in Section 2.3 is missing.

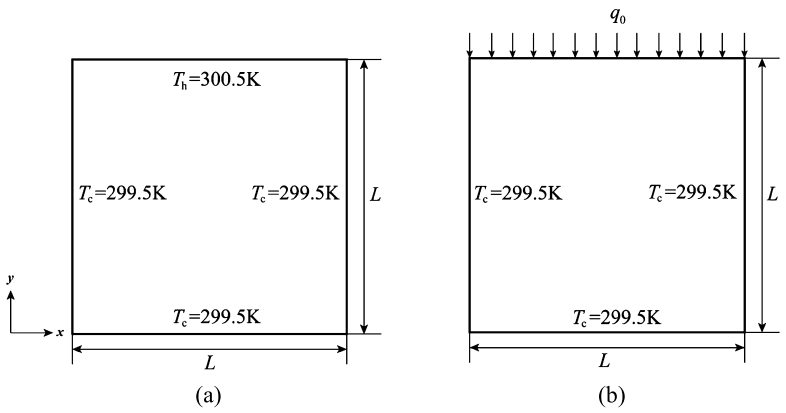

Fig. 5. Schematics of 2D steady-state phonon transport: (a) given temperature for the hot top, referred as case I and (b) given heat flux for the hot top, referred as case II.

3.2. Two-dimensional steady-state phonon transport

2D steady-state phonon transport is simulated in a region initially at a uniform temperature $T_c = 299.5$ K. Two cases as shown in Fig. 5(a) (case I) [40] and Fig. 5(b) (case II) [39] are considered. In case I, the top wall is prescribed at a given temperature $T_h = 300.5$ K; in case II, an inflowing heat flux $q_0 = 10^8$ W/m^2 is given. Such a magnitude of heat flux is exerted that the temperature rise is adequate to keep the average temperature in the whole region at about 300 K. The other three walls in both cases keep the initial temperature. Steady-state profiles of temperature and heat flux distribution will be reached after sufficiently long time. For both cases, phonon transport in the diffusive regime $Kn = l/L = 0.005$ is studied; the D2Q8 lattice is applied with a lattice speed $2v_g/3$ and grid numbers of 201×201 for case I, 301×301 for case II are chosen after grid independence verifications.

The expressions of steady-state temperature and heat flux distributions for case I are obtained through an analytical solution of Eq. (17) and Eq. (18) by the method of variable separation:

$$\begin{aligned}
\Theta(X,Y) &= \sum_{n=1}^{\infty} \frac{2[1-\cos(n\pi)]}{n\pi \sinh(n\pi)} \sin(n\pi X)\sinh(n\pi Y) \\
Q_x(X,Y) &= \sum_{n=1}^{\infty} \frac{2[1-\cos(n\pi)]}{\sinh(n\pi)} \cos(n\pi X)\sinh(n\pi Y) \\
Q_y(X,Y) &= \sum_{n=1}^{\infty} \frac{2[1-\cos(n\pi)]}{\sinh(n\pi)} \sin(n\pi X)\cosh(n\pi Y).
\end{aligned} \tag{27}$$

In Eq. (27), the non-dimensional coordinates, temperature and heat flux are defined respectively as:

$$X = \frac{x}{L}, \qquad Y = \frac{y}{L}, \qquad \Theta = \frac{T - T_c}{T_h - T_c}, \qquad Q = \frac{qL}{\lambda(T_c - T_h)}. \tag{28}$$

The steady-state analytical solutions for case II are obtained by the same method:

$$\begin{aligned}
\Theta(X,Y) &= \sum_{n=1}^{\infty} \frac{2Q_0}{(n\pi)^2} \frac{1-\cos n\pi}{\cosh n\pi} \sin(n\pi X)\sinh(n\pi Y) \\
Q_x(X,Y) &= -\sum_{n=1}^{\infty} \frac{2Q_0}{n\pi} \frac{1-\cos n\pi}{\cosh n\pi} \cos(n\pi X)\sinh(n\pi Y) \\
Q_y(X,Y) &= -\sum_{n=1}^{\infty} \frac{2Q_0}{n\pi} \frac{1-\cos n\pi}{\cosh n\pi} \sin(n\pi X)\cosh(n\pi Y).
\end{aligned} \tag{29}$$

The non-dimensional coordinates in Eq. (29) are the same as those in Eq. (28), while the non-dimensional temperature and heat flux in Eq. (29) are slightly different from those in Eq. (28):

$$\Theta = \frac{T - T_c}{T_c} \frac{1}{Kn}, \qquad Q = \frac{qL}{\lambda T_c} \frac{1}{Kn}. \tag{30}$$

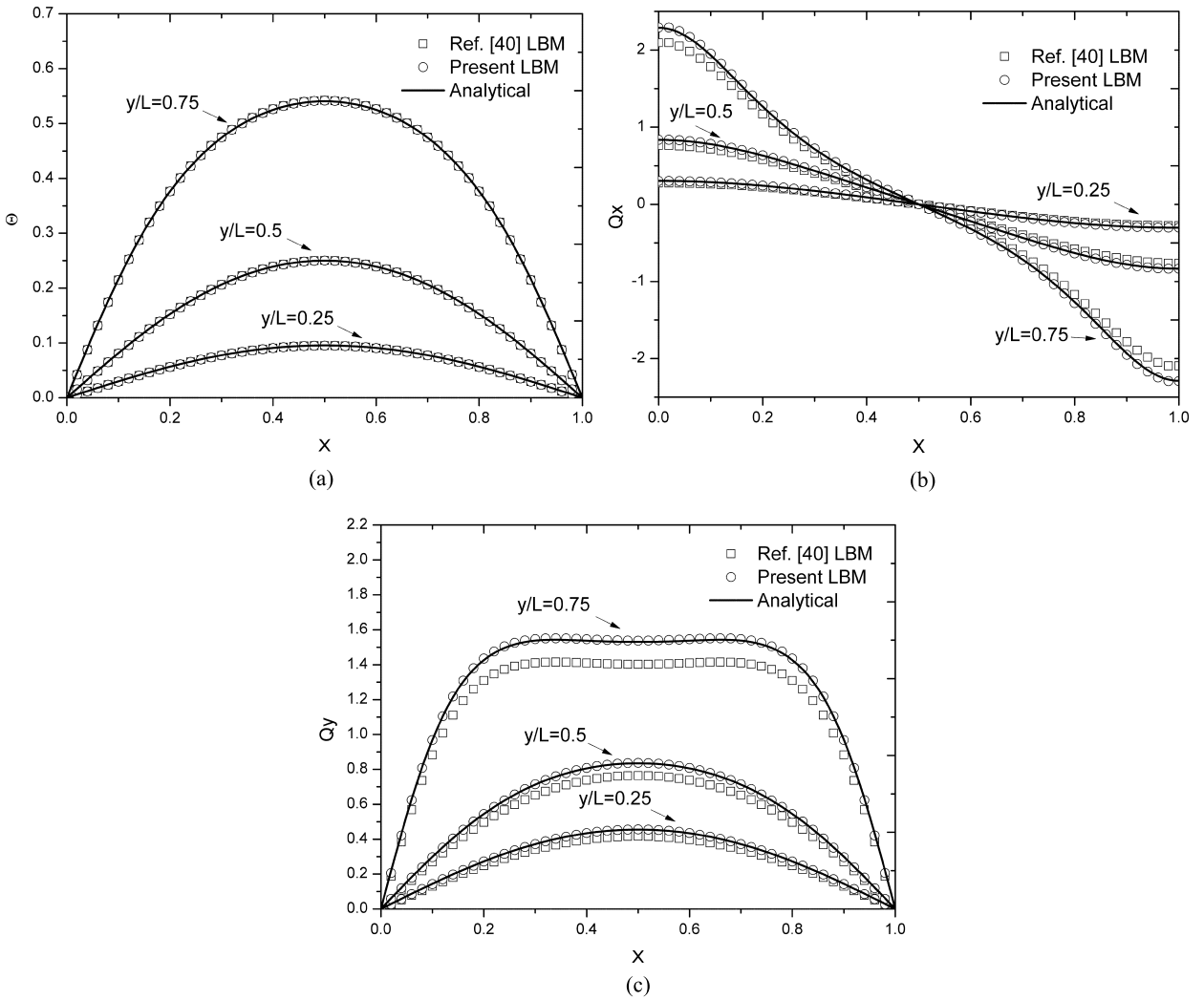

Fig. 6. Non-dimensional temperature and heat flux distributions in 2D steady-state phonon transport (case I): (a) temperature, (b) x-direction heat flux and (c) y-direction heat flux along the cross-sections at $y/L = 0.25$, 0.5 and 0.75 respectively. For the present LBM simulations, we use a grid of 201×201, D2Q8 with a lattice speed $c = 2v_g/3$. For comparison of the LBM modeling of Ref. [40], a grid of 201×201, D2Q8 with a lattice speed $c = 2v_g/\pi$ is used. The squares represent the numerical results by LBM in Ref. [40], the circles are the results by the present LBM, and the solid lines are the analytical solutions by Eq. (27).

The numerical results of the steady-state temperature and heat flux distributions for case I are shown in Fig. 6(a) and Fig. 6(b), (c) respectively. Further a comparison is made for case I between the results by the present lattice Boltzmann scheme and the previous scheme proposed in Ref. [40], where an empirical effective phonon group speed of $2v_g/\pi$ and identical weights of equilibrium distribution are used. The temperature distribution is predicted satisfactorily by the scheme proposed in Ref. [40], whereas the heat flux distribution is slightly underestimated. The numerical results of the steady-state temperature and heat flux distributions for case II are shown in Fig. 7(a)–(c), whose profiles are similar to those in case I. Note that the sign of the heat fluxes in case II are different from those in case I, because of the different non-dimensional variables. It is seen that a perfect agreement is achieved between the present lattice Boltzmann simulations and analytical solutions for both the temperature and heat flux distributions.

3.3. Three-dimensional steady-state phonon transport

3D steady-state phonon transport in a cubic region initially at a uniform temperature $T_c = 299.5$ K is studied. The top wall is prescribed at a given temperature $T_h = 300.5$ K, as is shown in Fig. 8. Thus steady-state profiles of temperature and heat flux distributions will be attained after sufficiently long time. Phonon transport in the diffusive regime $Kn = 0.01$ is studied; the D3Q14 lattice is applied with a lattice speed $\sqrt{\frac{7}{15}}v_g$ and a grid number $101 \times 101 \times 101$ is chosen after grid independence verifications.

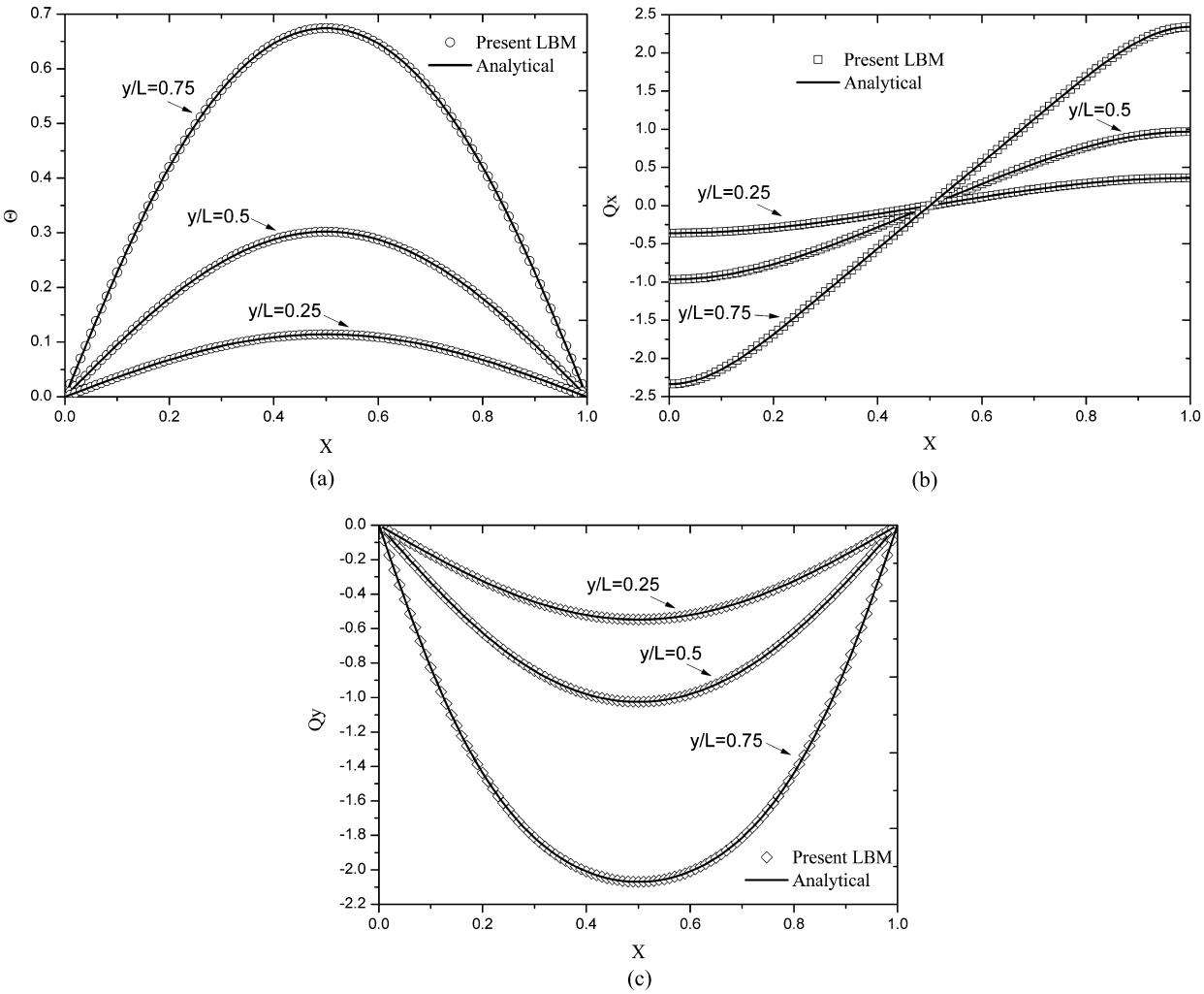

Fig. 7. Non-dimensional temperature and heat flux distributions in 2D steady-state phonon transport (case II): (a) temperature, (b) x-direction heat flux and (c) y-direction heat flux along the cross-sections at $y/L = 0.25$, 0.5 and 0.75 respectively. For the present LBM, a grid of 301×301, D2Q8 with lattice speed $c = 2v_g/3$ is used. The symbols represent the results by present LBM while solid lines are the analytical solutions by Eq. (29).

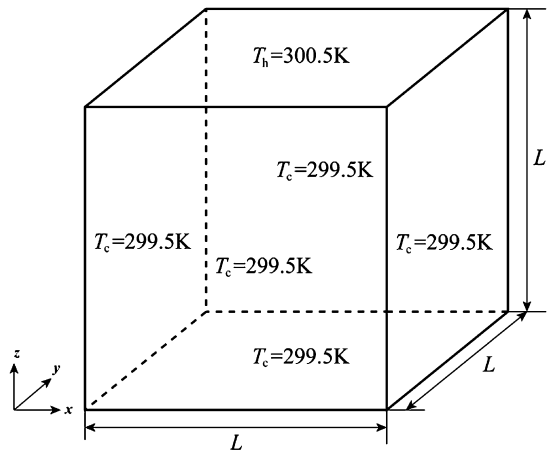

Fig. 8. Schematic of 3D steady-state phonon transport.

The expressions of temperature and heat flux distributions are got through an analytical solution of the heat diffusion equation by the method of variable separation:

$$\Theta(X,Y,Z)=\sum_{n=1}^{\infty}\sum_{m=1}^{\infty}\frac{4[1-\cos(n\pi)][1-\cos(m\pi)]}{mn\pi^2\sinh(\mu_{nm})}\sin(n\pi X)\sin(m\pi Y)\sinh(\mu_{nm}Z)$$

$$Q_x(X,Y,Z)=\sum_{n=1}^{\infty}\sum_{m=1}^{\infty}\frac{4[1-\cos(n\pi)][1-\cos(m\pi)]}{m\pi\sinh(\mu_{nm})}\cos(n\pi X)\sin(m\pi Y)\sinh(\mu_{nm}Z)$$

$$Q_y(X,Y,Z)=\sum_{n=1}^{\infty}\sum_{m=1}^{\infty}\frac{4[1-\cos(n\pi)][1-\cos(m\pi)]}{n\pi\sinh(\mu_{nm})}\sin(n\pi X)\cos(m\pi Y)\sinh(\mu_{nm}Z)$$

$$Q_z(X,Y,Z)=\sum_{n=1}^{\infty}\sum_{m=1}^{\infty}\frac{4\mu_{nm}[1-\cos(n\pi)][1-\cos(m\pi)]}{mn\pi^2\sinh(\mu_{nm})}\sin(n\pi X)\sin(m\pi Y)\cosh(\mu_{nm}Z), \tag{31}$$

with $\mu_{nm}=\sqrt{n^2+m^2}\pi$, $Z=z/L$, whereas other non-dimensional variables are the same as those in Eq. (28).

The numerical results of steady-state temperature and heat flux distributions are compared to the analytical solutions in Fig. 9(a), Fig. 9(b), Fig. 9(c) respectively. Since the behaviors of phonon transport in the x-direction are symmetrical to that in the y-direction, thus only the x-direction and z-direction heat fluxes are displayed. Again the present phonon lattice Boltzmann model gives an accurate prediction of both temperature and heat flux distributions in 3D steady-state phonon transport.

3.4. In-plane and cross-plane high-Kn phonon transport

Phonon transport across and through silicon thin films are studied here, as is shown in Fig. 10. The thickness of the thin film is H, and the Knudsen number is defined as $Kn=l/H$. The length and width of the thin film are much larger than the thickness, and therefore the cross-plane phonon transport reduces to a 1D problem, driven by the given wall temperatures $T_L=300.5$ K and $T_R=299.5$ K. Periodic boundary conditions are applied on the top and bottom boundaries for the cross-plane case. For the in-plane case, the walls are assumed adiabatic. A uniform temperature gradient is implemented along the in-plane direction by the periodic temperature gradient treatment provided in Section 2.4 to reduce the grid number for high Kn, where the simulation domain may become extremely non-uniform with a large length-thickness ratio. The D2Q8 lattice is used with a lattice speed $2v_g/3$ for both cases. A grid number of 1001×6 and 201×201 are applied for the cross-plane and in-plane cases respectively, after the grid independence verification.

The analytical results of cross-plane and in-plane phonon transports have been achieved through a solution of the phonon Boltzmann equation with gray relaxation time approximation. The effective thermal conductivity is therefore calculated based on the classical Fourier's law: $\lambda_{\text{eff}}=\frac{qH}{T_L-T_R}$ for the cross-plane case, and $\lambda_{\text{eff}}=\frac{L}{(T_L-T_R)}\frac{1}{H}\int_0^H q\,dy$ for the in-plane case. The cross-plane effective thermal conductivity available in all ranges of Kn was achieved based on the equation of phonon radiative transfer (EPRT) [52]:

$$\frac{\lambda_{\text{eff}}}{\lambda}=\frac{1}{1+\frac{4}{3}Kn}. \tag{32}$$

The in-plane effective thermal conductivity available in all ranges of Kn was achieved through an analytical solution of phonon Boltzmann equation with the diffuse boundary condition on lateral walls [1]:

$$\frac{\lambda_{\text{eff}}}{\lambda}=1-\frac{3}{8\eta}\left[1-4\left(E_3(\eta)-E_5(\eta)\right)\right], \tag{33}$$

with $\eta=1/Kn$, and the nth-order exponential integral $E_n(\eta)=\int_0^1\mu^{n-2}\exp(-\frac{\eta}{\mu})d\mu$. Eq. (33) is a special case of the classical Fuchs–Sondheimer model with a vanishing specularity parameter (cf. Eq. (111) in Ref. [5]).

The numerical results of cross-plane and in-plane effective thermal conductivity by the present lattice Boltzmann scheme are compared to the analytical solutions in Fig. 11(a) and Fig. 11(b) respectively. For the cross-plane case shown in Fig. 11(a), the lattice Boltzmann simulation displays a perfect agreement with the analytical solution of Eq. (32) in a large range of Kn. With Kn increasing, the effective thermal conductivity decreases because of the size effect. A linear temperature distribution is attained across the thin film with temperature jumps observed at the boundaries, which agree quantitatively with previous available results through a solution of EPRT by discrete-ordinate method [52], as is shown in Fig. 12. For the in-plane case shown in Fig. 11(b), the lattice Boltzmann prediction agrees well with the analytical solution of Eq. (33) when $Kn <\sim 1$. For higher Kn the present predictions overate the effective thermal conductivity. The reason lies in that the continuum assumption for the classical Fourier's law breaks down when Kn is high. Similar problems have also been met in lattice Boltzmann modeling of microscale gas flow, where the fluid behavior was captured satisfactorily only in the hydrodynamic regime (negligible Kn effects) without modifications to the original BGK scheme [27,53]. In order to remedy

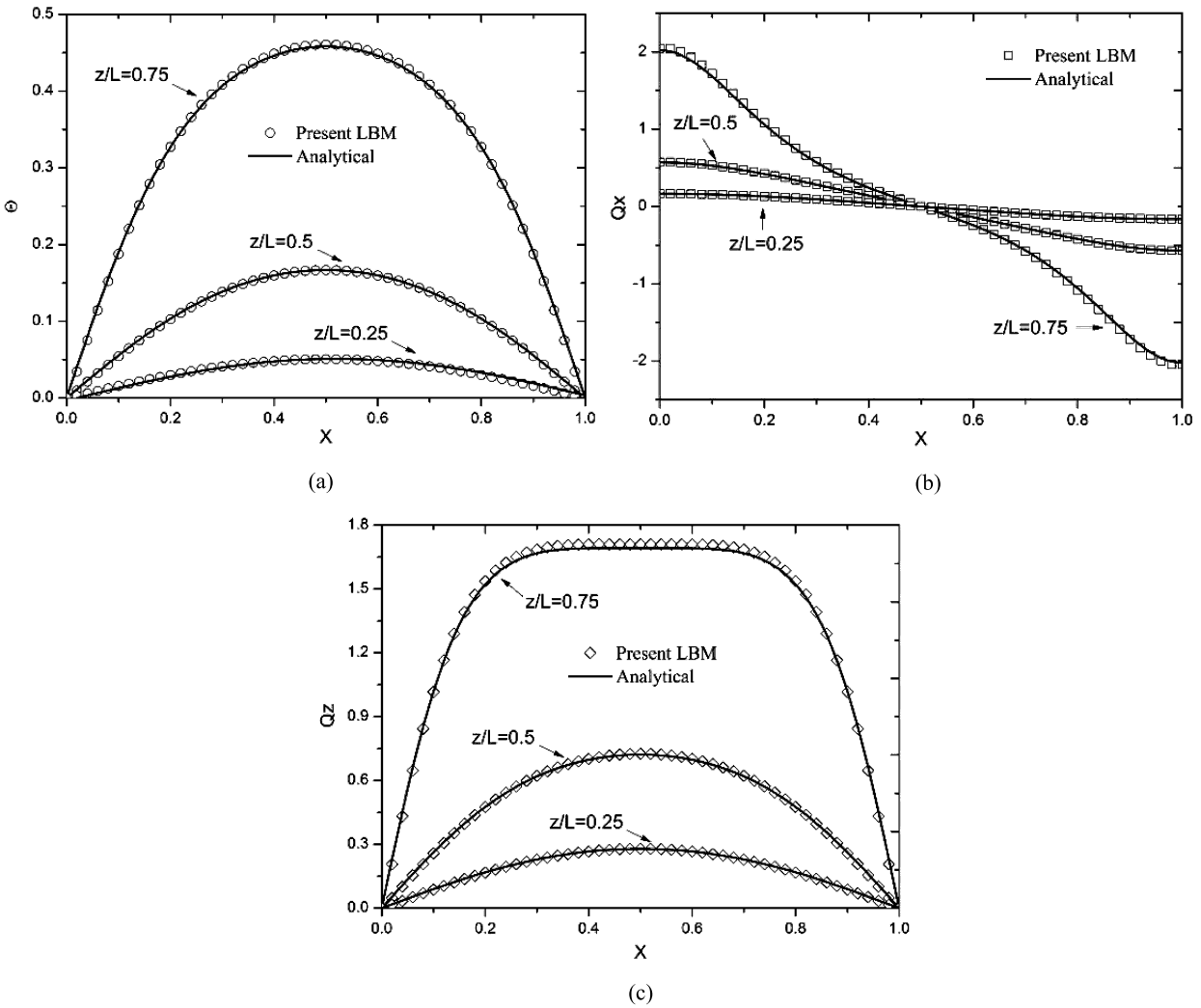

Fig. 9. Non-dimensional temperature and heat flux distributions in 3D steady-state phonon transport in the mid-plane ($y/L = 0.5$): (a) temperature, (b) x-direction heat flux and (c) z-direction heat flux along the cross-sections at $z/L = 0.25$, 0.5 and 0.75 respectively. For the present LBM, a grid of $101 \times 101 \times 101$, D3Q14 with lattice speed $c = \sqrt{\frac{7}{15}} v_g$ is used. The symbols represent the results by present LBM while solid lines are the analytical solutions by Eq. (31).

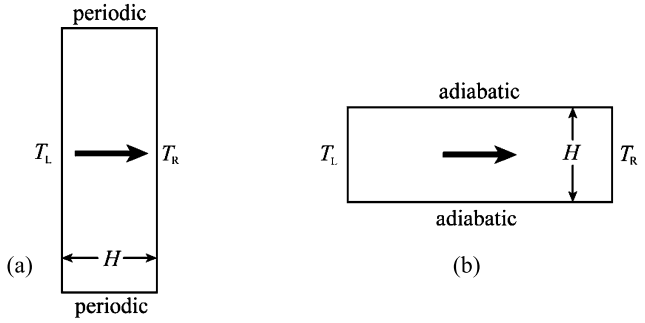

Fig. 10. Phonon transport in a thin film with a thickness of H along different heat flux directions: (a) cross-plane direction; (b) in-plane direction.

the situation, an effective relaxation time correction is introduced into the lattice Boltzmann scheme, $\tau_{\text{eff}} = \tau \frac{1}{1+\alpha Kn}$, inspired by the effective viscosity model in the lattice Boltzmann model for the microscale gas flows [54]. This modification indicates a corrected mean free path (l) in a confined space by walls correlated to the high Kn situation. The relaxation time τ_R is

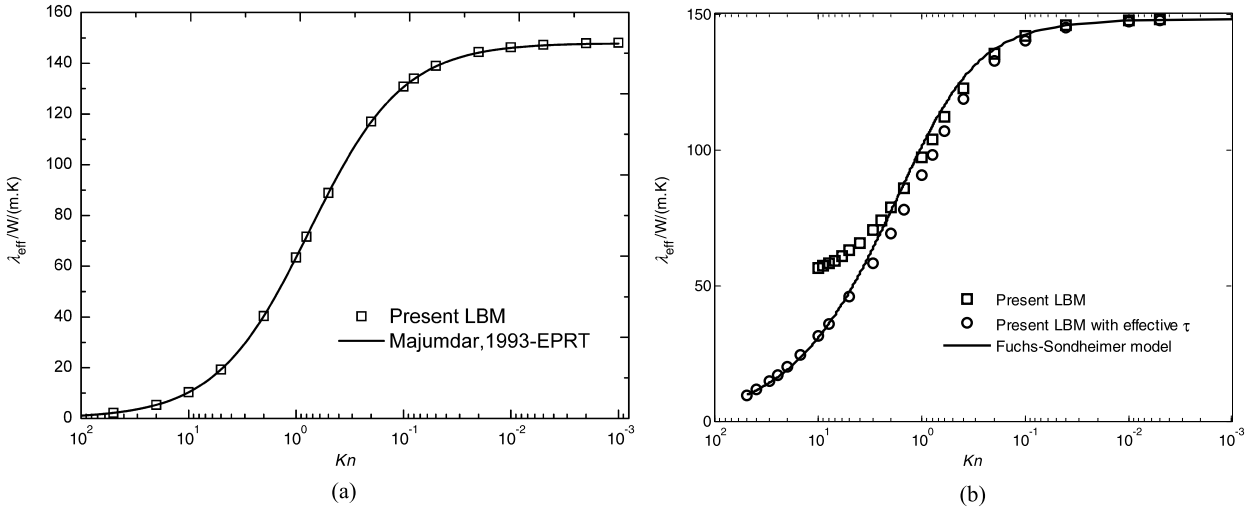

Fig. 11. Effective thermal conductivities of silicon thin film versus *Kn* at 300 K for: (a) cross-plane case and (b) in-plane case. The squares represent the numerical result by the present LBM, the cycles in (b) represent the numerical results with a modified effective relaxation time, and the solid lines represent analytical results.

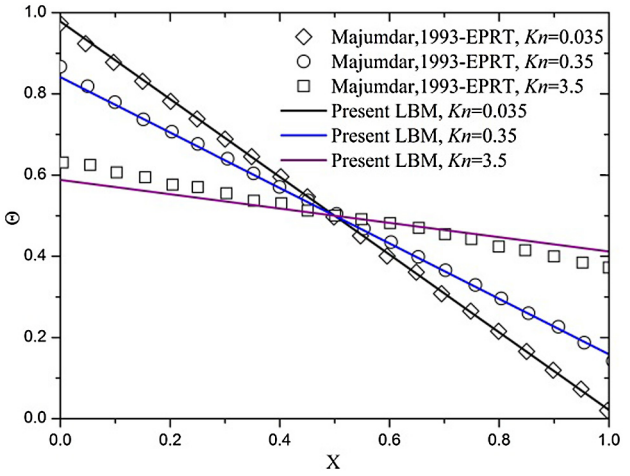

Fig. 12. Dimensionless temperature profiles in the cross-plane case: the symbols represent results from solution of EPRT in Ref. [52], the solid lines represent the results by present LBM. The dimensionless temperature is defined as: $\Theta = (T - T_R)/(T_L - T_R)$.

therefore modified through $l = \tau_R v_g$. The empirical coefficient $\alpha = 0.1$ is obtained by adjusting the numerical results to the analytical solution. Thus, the present lattice Boltzmann scheme is extended to model in-plane phonon transport at higher *Kn* beyond its original scope.

In summary, the present phonon lattice Boltzmann method works well for predicting phonon transport in the diffusive regime, and gives satisfactory results in the regime not too far from the diffusive regime ($Kn \leq \sim 1$). The proposed D2Q8 lattice scheme eliminates the fictitious phonon speed in the diagonal direction of a square lattice system in previous lattice Boltzmann models. With the correct correspondences between numerical parameters and material properties, the lattice resolution is greatly reduced from about fifty [40] to one lattice per phonon mean free path to accurately capture the temperature and heat flux profiles of both steady-state and transient phonon transports. Further work is still pending to rigorously extend the present lattice Boltzmann scheme to model nanoscale phonon transport, where *Kn* is extremely high and the nonlocal effect is dominant (cf. Ref. [5] and the references therein). Although previous work [55] has made some effort in modeling the nonlocal effects based on a lattice Boltzmann scheme of phonon hydrodynamics, a solid connection is still lacking between the mesoscopic algorithm and macroscopic equation for nanoscale phonon transport, as is summarized thoroughly in Section 5.3 of Ref. [5]. Another challenge in phonon lattice Boltzmann modeling is the accurate description of phonon-boundary (interfacial) interaction, which becomes increasingly pertinent in nanosystems.

4. Conclusions

The present work establishes a theoretical foundation for the proposed phonon lattice Boltzmann scheme. The numerical parameters are rigorously correlated to the bulk material properties based on a Chapman–Enskog expansion to phonon lattice Boltzmann equation, so that all of the inconsistencies in previous work are naturally removed. Both the steady-state and transient, one-dimensional and multi-dimensional phonon transport can be modeled accurately by the new scheme in the diffusive regime. After relaxation time modification, the present phonon lattice Boltzmann method works well for predicting phonon transport in a wider range of *Kn*. The linear and gray approximations in this work remains to be generalized by including the actual phonon dispersion relation and frequency-dependent relaxation time in future work. Modeling phonon transport in nanosystems with complex geometries by the present lattice Boltzmann scheme will be explored soon, which may provide a deeper understanding of nonlinear and nonlocal heat transports at nanoscale and an efficient way to optimize heat transfer pathways in nanodevices.

Acknowledgements

The authors appreciate helpful discussions with C.Y. Xie and K. Luo. This work is financially supported by the NSFC grant (Nos. 51176089, 51321002, U1562217), the Key Basic Scientific Research Program (2013CB228301) and the Tsinghua University Initiative Scientific Research Program.

References

[1] G. Chen, Nanoscale Energy Transport and Conversion: A Parallel Treatment of Electrons, Molecules, Phonons, and Photons, Oxford University Press, New York, 2005.
[2] M. Kaviany, Heat Transfer Physics, Cambridge University Press, New York, 2008.
[3] D.G. Cahill, P.V. Braun, G. Chen, D.R. Clarke, S. Fan, K.E. Goodson, P. Keblinski, W.P. King, G.D. Mahan, A. Majumdar, H.J. Maris, S.R. Phillpot, E. Pop, L. Shi, Nanoscale thermal transport. II. 2003–2012, Appl. Phys. Rev. 1 (2014) 011305.
[4] A.J. Minnich, Advances in the measurement and computation of thermal phonon transport properties, J. Phys. Condens. Matter 27 (2015) 053202.
[5] Y. Guo, M. Wang, Phonon hydrodynamics and its applications in nanoscale heat transport, Phys. Rep. 595 (2015) 1–44.
[6] N. Yang, G. Zhang, B. Li, Violation of Fourier's law and anomalous heat diffusion in silicon nanowires, Nano Today 5 (2010) 85–90.
[7] A.J.H. McGaughey, J.M. Larkin, Predicting phonon properties from equilibrium molecular dynamics simulations, Annu. Rev. Heat Transf. 17 (2014) 49–87.
[8] R.E. Peierls, Quantum Theory of Solids, The Clarendon Press, Oxford, 1955.
[9] J. Fourier, Théorie analytique de la chaleur, Firmin Didot Père et Fils, Paris, 1822.
[10] D. Jou, J. Casas-Vázquez, G. Lebon, Extended Irreversible Thermodynamics, Springer, Heidelberg, 2010.
[11] C. Cattaneo, Sulla conduzione del calore, Atti Semin. Mat. Fis. Univ. Modena 3 (1948) 21.
[12] P. Vernotte, Les paradoxes de la théorie continue de l'équation de la chaleur, C. R. Acad. Sci. 246 (1958) 3154–3155.
[13] D.D. Joseph, L. Preziosi, Heat waves, Rev. Mod. Phys. 61 (1989) 41–73.
[14] B. Straughan, Heat Waves, Springer, New York, 2011.
[15] E.P. Scott, M. Tilahun, B. Vick, The question of thermal waves in heterogeneous and biological materials, J. Biomech. Eng. 131 (2009) 074518.
[16] F.X. Alvarez, D. Jou, A. Sellitto, Phonon hydrodynamics and phonon-boundary scattering in nanosystems, J. Appl. Phys. 105 (2009) 014317.
[17] D. Jou, G. Lebon, M. Criado-Sancho, Variational principles for thermal transport in nanosystems with heat slip flow, Phys. Rev. E 82 (2010) 031128.
[18] D.Y. Tzou, Macro- to Microscale Heat Transfer: The Lagging Behavior, John Wiley & Sons, Ltd., Chichester, 2015.
[19] M. Wang, N. Yang, Z.-Y. Guo, Non-Fourier heat conductions in nanomaterials, J. Appl. Phys. 110 (2011) 064310.
[20] F.X. Alvarez, V.A. Cimmelli, D. Jou, A. Sellitto, Mesoscopic description of boundary effects in nanoscale heat transport, Nanoscale Syst. MMTA 1 (2012) 112–142.
[21] J.-P.M. Peraud, C.D. Landon, N.G. Hadjiconstantinou, Monte Carlo methods for solving the Boltzmann equation, Annu. Rev. Heat Transf. 17 (2014) 205–265.
[22] G. Chen, Multiscale simulation of phonon and electron thermal transport, Annu. Rev. Heat Transf. 17 (2014) 1–8.
[23] S. Succi, The Lattice Boltzmann Equation for Fluid Dynamics and Beyond, Clarendon Press, Oxford, 2001.
[24] Z.L. Guo, C. Shu, Lattice Boltzmann Method and Its Applications in Engineering, World Scientific Publishing, Singapore, 2013.
[25] H.D. Chen, S.Y. Chen, W.H. Matthaeus, Recovery of the Navier–Stokes equations using a lattice–gas Boltzmann method, Phys. Rev. A 45 (1992) R5339–R5342.
[26] X.Y. He, L.S. Luo, Theory of the lattice Boltzmann method: from the Boltzmann equation to the lattice Boltzmann equation, Phys. Rev. E 56 (1997) 6811–6817.
[27] S.Y. Chen, G.D. Doolen, Lattice Boltzmann method for fluid flows, Annu. Rev. Fluid Mech. 30 (1998) 329–364.
[28] X.W. Shan, G. Doolen, Diffusion in a multicomponent lattice Boltzmann equation model, Phys. Rev. E 54 (1996) 3614–3620.
[29] J.K. Wang, M. Wang, Z.X. Li, Lattice Poisson–Boltzmann simulations of electro-osmotic flows in microchannels, J. Colloid Interface Sci. 296 (2006) 729–736.
[30] J. Wang, M. Wang, Z. Li, A lattice Boltzmann algorithm for fluid–solid conjugate heat transfer, Int. J. Therm. Sci. 46 (2007) 228–234.
[31] J. Zhang, G. Yan, X. Shi, Lattice Boltzmann model for wave propagation, Phys. Rev. E 80 (2009) 026706.
[32] Y. Ma, S.K. Dong, H.P. Tan, Lattice Boltzmann method for one-dimensional radiation transfer, Phys. Rev. E 84 (2011) 016704.
[33] S.S. Ghai, W.T. Kim, R.A. Escobar, C.H. Amon, M.S. Jhon, A novel heat transfer model and its application to information storage systems, J. Appl. Phys. 97 (2004) 10P703.
[34] J. Xu, X.W. Wang, Simulation of ballistic and non-Fourier thermal transport in ultra-fast laser heating, Physica B 351 (2004) 213–226.
[35] W.S. Jiaung, J.R. Ho, Lattice Boltzmann study on size effect with geometrical bending on phonon heat conduction in a nanoduct, J. Appl. Phys. 95 (2004) 958–966.
[36] R.A. Escobar, S.S. Ghai, M.S. Jhon, C.H. Amon, Multi-length and time scale thermal transport using the lattice Boltzmann method with application to electronics cooling, Int. J. Heat Mass Transf. 49 (2006) 97–107.
[37] R.A. Escobar, C.H. Amon, Influence of phonon dispersion on transient thermal response of silicon-on-insulator transistors under self-heating conditions, J. Heat Transf. 129 (2007) 790–797.
[38] R.A. Escobar, C.H. Amon, Thin film phonon heat conduction by the dispersion lattice Boltzmann method, J. Heat Transf. 130 (2008) 092402.

[39] A. Christensen, S. Graham, Multiscale lattice Boltzmann modeling of phonon transport in crystalline semiconductor materials, Numer. Heat Transf., Part B, Fundam. 57 (2010) 89–109.
[40] A. Nabovati, D.P. Sellan, C.H. Amon, On the lattice Boltzmann method for phonon transport, J. Comput. Phys. 230 (2011) 5864–5876.
[41] P. Heino, Lattice-Boltzmann finite-difference model with optical phonons for nanoscale thermal conduction, Comput. Math. Appl. 59 (2010) 2351–2359.
[42] D.P. Sellan, J.E. Turney, A.J.H. McGaughey, C.H. Amon, Cross-plane phonon transport in thin films, J. Appl. Phys. 108 (2010) 113524.
[43] Y.F. Han, X.L. Xia, H.P. Tan, H.D. Liu, Modeling of phonon heat transfer in spherical segment of silica aerogel grains, Physica B 420 (2013) 58–63.
[44] A. Chattopadhyay, A. Pattamatta, A comparative study of submicro phonon transport using the Boltzmann transport equation and the lattice Boltzmann method, Numer. Heat Transf., Part B, Fundam. 66 (2014) 360–379.
[45] Y.F. Han, X.L. Xia, H.D. Liu, Size effect of phonon heat transport in nanomaterial for square structure, J. Comput. Theor. Nanosci. 11 (2014) 702–705.
[46] A. Chattopadhyay, A. Pattamatta, Energy transport across submicron porous structures: a lattice Boltzmann study, Int. J. Heat Mass Transf. 72 (2014) 479–488.
[47] Y. Mao, M. Xu, Lattice Boltzmann numerical analysis of heat transfer in nano-scale silicon films induced by ultra-fast laser heating, Int. J. Therm. Sci. 89 (2015) 210–221.
[48] R.S. Samian, A. Abbassi, J. Ghazanfarian, Transient conduction simulation of a nano-scale hotspot using finite volume lattice Boltzmann method, Int. J. Mod. Phys. C 25 (2014) 1350103.
[49] S. Chapman, T.G. Cowling, The Mathematical Theory of Non-uniform Gases, Cambridge University Press, Cambridge, 1953.
[50] Q. Hao, G. Chen, M.-S. Jeng, Frequency-dependent Monte Carlo simulations of phonon transport in two-dimensional porous silicon with aligned pores, J. Appl. Phys. 106 (2009) 114321.
[51] D.W. Hahn, M.N. Özisik, Heat Conduction, John Wiley & Sons, Inc., Hoboken, 2012.
[52] A. Majumdar, Microscale heat conduction in dielectric thin films, J. Heat Transf. 115 (1993) 7–16.
[53] X. Nie, G.D. Doolen, S. Chen, Lattice-Boltzmann simulations of fluid flows in MEMS, J. Stat. Phys. 107 (2002) 279–289.
[54] A. Homayoon, A.H.M. Isfahani, E. Shirani, M. Ashrafizadeh, A novel modified lattice Boltzmann method for simulation of gas flows in wide range of Knudsen number, Int. Commun. Heat Mass Transf. 38 (2011) 827–832.
[55] W.-S. Jiaung, J.-R. Ho, Lattice-Boltzmann modeling of phonon hydrodynamics, Phys. Rev. E 77 (2008) 066710.